Inorganic Chemistry

Article

Synthetic and Computational Studies on Factors Controlling Structures of Molecular Triangles and Squares and Their Equilibrium in Solutions

Kazuhiro Uehara,[†,‡] Ko Kasai,[†] and Noritaka Mizuno[*,†,‡]

[†]*Department of Applied Chemistry, School of Engineering, The University of Tokyo, 7-3-1 Hongo, Bunkyo-ku, Tokyo 113-8656, Japan, and* [‡]*Core Research for Evolutional Science and Technology* (*CREST*), *Japan Science and Technology Agency* (*JST*), *4-1-8 Honcho, Kawaguchi, Saitama 332-0012, Japan*

Reactions of (en*)Pd(NO$_3$)$_2$ (en* = N,N,N',N'-tetramethylethylenediamine) with a series of organic bridging ligands of pyrazine, 1,2-bis(4-pyridyl)ethylene, 1,2-bis(4-pyridyl)acetylene, and 1,4-bis(4-pyridyl)benzene are carried out to investigate factors controlling the supramolecular structures and the equilibrium between the molecular triangles and the squares in solutions. The molecular structures of solid triangular [(en*)Pd(L$_n$)]$_3$(NO$_3$)$_6$ with 1,2-bis(4-pyridyl)ethylene and 1,2-bis(4-pyridyl)acetylene bridging ligands are determined by X-ray crystallography: [(en*)Pd(1,2-bis(4-pyridyl)ethylene)]$_3$(NO$_3$)$_6$, monoclinic Pn (No. 7), a = 17.3242(3) Å, b = 15.0804(3) Å, c = 17.3223(3) Å, β = 103.5100(10)°, V = 4400.33(14) Å^3, Z = 2; [(en*)Pd(1,2-bis(4-pyridyl)acetylene)]$_3$(NO$_3$)$_6$, orthorhombic $Aba2$ (No. 41), a = 14.6642(3) Å, b = 27.8763(5) Å, c = 21.4233(4) Å, V = 8757.5(3) Å^3, Z = 4. In contrast, an infinite chain structure of {[(en*)Pd(pyrazine)](NO$_3$)}$_\infty$ (monoclinic $P2_1/m$ (No. 11), a = 14.4740(7) Å, b = 8.9209(3) Å, c = 28.9705(13) Å, β = 89.974(2)°, V = 3740.7(3) Å^3, Z = 2) is observed with the shortest pyrazine. The steric hindrance between the supporting and the bridging ligands or the neighboring supporting ligands would contribute to the formation of the infinite chain complex **1**. The N(Py)–Pd–N(Py) angles in the solid molecular triangles monotonically increased closely to 90° with the increase in the lengths of the bridging ligands, indicating the relaxation of the steric hindrance between the supporting and the bridging ligands. The structures of the molecular triangles and squares in solutions are optimized with density functional theory (DFT) calculations using the conductor-like polarizable continuum model (C-PCM), and the resulting structures are almost the same as those in the solid state. The ^{1}H NMR spectra indicate that (i) the equilibrium between the molecular triangles and the squares is attained upon the introduction of the methyl substituents into the en supporting ligands (en*), (ii) the $\Delta G°$ values decreased with the increase in the lengths of the straight bridging ligands, and (iii) the equilibrium constants depend on the kinds of solvents. The ^{1}H NMR spectra estimated with the gauge invariant atomic orbital DFT (GIAO–DFT) calculations well reproduce the experimental data, and the single-point energy DFT calculations with C-PCM in the presence of the solvents approximately reproduce the facts (i)–(iii).

Introduction

In nature, enzymes fascinatingly fabricate the selective recognition sites of specific molecules with the aid of the external stimuli, weak chemical interactions or surrounded environments.[1] The molecular recognition plays an important role in the life activity of various creatures. The diverse and intrinsic functions have attracted much attention and lead to recent developments of supramolecular chemistry.[2] The supramolecules can be synthesized by the self-assembly using weak hydrogen bonding, electrostatic, and coordination interactions

and exhibit the specific molecular recognition utilizing the well-organized nanosized spaces. One of the simplest examples is a molecular polygon.[3] These compounds often exist as equilibrium mixtures of molecular triangles and squares or molecular rhomboids and hexagons in solvents.[4−25]

*To whom correspondence should be addressed. E-mail: tmizuno@mail.ecc.u-tokyo.ac.jp. Phone: +81-3-5841-7272. Fax: +81-3-5841-7220.

(1) The thematic issue on bioinorganic chemistry: (a) Holm, R. H., Solomon, E. I., Eds.; *Chem. Rev.* **2004**, *104*, 347. (b) Holm, R. H, Solomon, E. I., Eds.; *Chem. Rev.* **1996**, *96*, 2237.

(2) (a) Lehn, J.-M. *Supramolecular Chemistry*; VCH: Weinheim, 1995. (b) *Supramolecular Organometallic Chemistry*, Haiduc I., Edelmann F. T., Eds.; VCH: Weinheim, 1999.

(3) (a) Stang, P. J.; Olenyuk, B. *Acc. Chem. Res.* **1997**, *30*, 502. (b) Fujita, M.; Tominaga, M.; Hori, A.; Therrien, B. *Acc. Chem. Res.* **2005**, *35*, 371. (c) Leininger, S.; Olenyuk, B.; Stang, P. J. *Chem. Rev.* **2000**, *100*, 853. (d) Amijs, C. H. M.; van Klink, G. P. M.; van Koten, G. *J. Chem. Soc., Dalton Trans.* **2006**, 308. (e) Zangrando, E.; Casanova, M.; Alessio, E. *Chem. Rev.* **2008**, *108*, 4979.
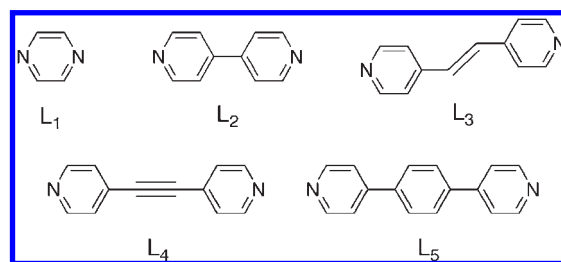
(4) (a) Fujita, M.; Sasaki, O.; Mitsuhashi, T.; Fujita, T.; Yazaki, J.; Yamaguchi, K.; Ogura, K. *J. Chem. Soc., Chem. Commun.* **1996**, 1535. (b) Fujita, M.; Yazaki, J.; Ogura, K. *J. Am. Chem. Soc.* **1990**, *112*, 5645. (c) Fujita, M.; Yazaki, J.; Ogura, K. *Tetrahedron Lett.* **1991**, *32*, 5589.

(5) (a) Schweiger, M.; Seidel, S. R.; Arif, A. M.; Stang, P. J. *Angew. Chem., Int. Ed.* **2001**, *40*, 3467. (b) Schweiger, M.; Seidel, R.; Arif, A. M.; Stang, P. J. *Inorg. Chem.* **2002**, *41*, 2556.

(6) Lai, S.-W.; Chan, M. C.-W.; Peng, S.-M.; Che, C.-W. *Angew. Chem., Int. Ed.* **1999**, *38*, 699.

The rational syntheses and structure controls are important research topics in supramolecular chemistry. As for the self-assembly reactions of the linear bridging ligands and 90° angular metal fragments to form the molecular triangles and squares, it is generally accepted that the molecular squares are enthalpically favored, whereas the molecular triangles are entropically preferred. It has also been accepted that in the *absence* of the steric hindrance between the supporting and the bridging ligands the molecular triangles become more favorable with the decrease in the rigidity and increase in the lengths of the bridging ligands.[3,4a] Moreover, the molecular triangles are favored at the low concentration according to the Le Châtelier's principle. However, the factors controlling the
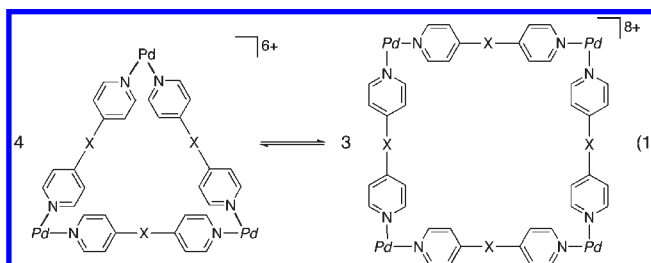
Chart 1

equilibrium between the molecular triangles and the squares have not yet been clarified.

There are few reports on the equilibrium from the viewpoints of both synthetic and computational chemistry. Ferrer et al. have reported that the changes in the Gibbs-free energies from the molecular squares $[(L')Pd(L)]_4(NO_3)_8$ (L' = ethylenediamine (en) and 1,3-bis(diphenylphosphino)propane (dppp), L = 1,4-bis(4-pyridyl)tetrafluorobenzene) to the corresponding molecular triangles are calculated to be about 602.5 and about 552.3 kJ mol^{-1}, respectively,[11] using the Universal Force Field with the molecular dynamics. This shows that only the molecular squares are present, while the molecular triangles are also present experimentally (the molecular square/triangle ratio = 7/3). Alessio et al. have also reported that the change in the internal energy from the molecular triangle [*trans,cis*-RuCl$_2$(DMSO-S)$_2$-(μ-L$_1$)]$_3$ (L$_1$ = pyrazine) to the corresponding molecular square using the density functional theory (DFT) calculations with the B3LYP/TZV level of theory under the vacuum conditions is −60.2 kJ mol^{-1}.[12] This shows that only the molecular square is present, while only the molecular triangle is observed experimentally. Therefore, the computational results have not yet rationally explained the equilibrium.

We have recently reported the syntheses of the molecular triangle $[(en^*)Pd(L_2)]_3(NO_3)_6$ **2a·NO$_3$** and square $[(en^*)Pd(L_2)]_4(NO_3)_8$ **2b·NO$_3$** (en* = N,N,N',N'-tetramethylethylenediamine, L$_2$ = 4,4'-bipyridine) and that the equilibrium constants in DMSO-d_6 and D$_2$O were different from each other (Chart 1).[13] In this article, we report the syntheses and characterizations of solid Pd-based molecular triangles with a series of organic bridging ligands of 1,2-bis(4-pyridyl)ethylene (L$_3$), 1,2-bis(4-pyridyl)acetylene (L$_4$), and 1,2-bis(4-pyridyl)benzene (L$_5$), and a solid Pd-based infinite chain complex $\{(en^*)Pd(L_1)(NO_3)_2\}_\infty$ **1** (Chart 1). In addition, the factors controlling the structures of the molecular triangles and squares $[(en^*)Pd(L_n)]_m(NO_3)_{2m}$ (m = 3, 4; n = 2−5) and the equilibrium in the solution (eq 1) are investigated with the ^{1}H NMR measurements and DFT calculations.

$$(1)$$

(7) (a) Schnebeck, R.-D.; Freisinger, E.; Glahé, F.; Lippert, B. *J. Am. Chem. Soc.* **2000**, *122*, 1381. (b) Willermann, M.; Mulcahy, C.; Sigel, R. K. O.; Cerdà, M. M.; Freisinger, E.; Miguel, P. J. S.; Roitzsch, M.; Lippert, B. *Inorg. Chem.* **2006**, *45*, 2093.
(8) Reference 8 was not submitted.
(9) Carina, R. F.; Williams, A. F.; Bernardinelli, G. *Inorg. Chem.* **2001**, *40*, 1826.
(10) Yu, S.-Y.; Huang, H.-P.; Li, S.-H.; Jiao, Q.; Li, Y.-Z.; Wu, B.; Sei, Y.; Yamaguchi, K.; Pan, Y.-J.; Ma, H.-W. *Inorg. Chem.* **2005**, *44*, 9471.
(11) (a) Ferrer, M.; Gutiérrez, A.; Mounir, M.; Rossell, O.; Ruiz, E.; Rang, A.; Engeser, M. *Inorg. Chem.* **2007**, *46*, 3395. (b) Ferrer, M.; Mounir, M.; Ruiz, E.; Maestro, M. A. *Inorg. Chem.* **2003**, *42*, 5890.
(12) Derossi, S.; Casanova, M.; Lengo, E.; Zangrando, E.; Stener, M.; Alessio, E. *Inorg. Chem.* **2007**, *46*, 11243.
(13) Uehara, K.; Kasai, K.; Mizuno, N. *Inorg. Chem.* **2007**, *46*, 2563.
(14) Weilandt, T.; Troff, R. W.; Saxell, H.; Rissanen, K.; Schalley, C. A. *Inorg. Chem.* **2008**, *47*, 7588.
(15) Lee, S. B.; Hwang, S.; Chung, D. S.; Yun, H.; Hong, J.-I. *Tetrahedron Lett.* **1998**, *39*, 873.
(16) (a) Hasenknopf, B.; Lehn, J.-M.; Boumediene, N.; Dupont-Gervais, A.; Van Dorsselaer, A.; Kneisel, B.; Fenske, D. *J. Am. Chem. Soc.* **1997**, *119*, 10956. (b) Ali, Md. M.; MacDonnell, F. M. *J. Am. Chem. Soc.* **2000**, *122*, 11527. (c) Stang, P. J.; Persky, N. E.; Manna, J. *J. Am. Chem. Soc.* **1997**, *119*, 4777. (d) Matsumoto, N.; Motoda, Y.; Matsuo, T.; Nagashima, T.; Re, N.; Dahan, F.; Tuchagues, J.-P. *Inorg. Chem.* **1999**, *38*, 1165. (e) Lai, S.-W.; Cheung, K.-K.; Chan, M. C.-W.; Che, C.-M. *Angew. Chem., Int. Ed.* **1998**, *37*, 182. (f) Saalfrank, R. W.; Bernt, I.; Uller, E.; Hampel, F. *Angew. Chem., Int. Ed. Engl.* **1997**, *36*, 2482. (g) Newkome, G. R.; Cho, T. J.; Moorefield, C. N.; Baker, G. R.; Cush, R.; Russo, P. S. *Angew. Chem., Int. Ed.* **1999**, *38*, 3717. (h) Mamula, O.; Monlien, J.; Porquet, A.; Hopfgartner, G.; Merbach, A. E.; von Zelewski, A. *Chem.—Eur. J.* **2001**, *7*, 533. (i) Kumazawa, K.; Biradha, T.; Kusukawa, K.; Okano, T.; Fujita, M. *Angew. Chem., Int. Ed.* **2003**, *42*, 3909. (j) Qin, Z.; Jennings, M. C.; Puddephatt, R. J. *Inorg. Chem.* **2002**, *41*, 3967.
(17) (a) Cotton, F. A.; Lin, C.; Murillo, C. A. *Acc. Chem. Res.* **2001**, *34*, 759. (b) Cotton, F. A.; Daniels, L. M.; Lin, C.; Murillo, C. A. *J. Am. Chem. Soc.* **1999**, *121*, 4538. (c) Cotton, F. A.; Lin, C.; Murillo, C. A. *Inorg. Chem.* **2001**, *40*, 575. (d) Cotton, F. A.; Murillo, C. A.; Yu, R. *J. Chem. Soc., Dalton Trans.* **2006**, 3900. (e) Cotton, F. A.; Liu, C. Y.; Murillo, C. A.; Wang, X. *Inorg. Chem.* **2006**, *45*, 2619. (f) Angaridis, P.; Berry, J. F.; Cotton, F. A.; Murillo, C. A.; Wang, X. *J. Am. Chem. Soc.* **2003**, *125*, 10327. (g) Cotton, F. A.; Murillo, C. A.; Wang, X.; Yu, R. *Inorg. Chem.* **2004**, *43*, 2004.
(18) (a) Sun, S.-S.; Lees, J. L. *Inorg. Chem.* **2001**, *40*, 3154. (b) Sun, S.-S.; Lees, A. J. *J. Am. Chem. Soc.* **2000**, *122*, 8956.
(19) (a) Berben, L. A.; Fara, M. C.; Crawford, N. R. M.; Long, J. R. *Inorg. Chem.* **2006**, *45*, 6378. (b) Lau, V. C.; Berben, L. A.; Long, J. R. *J. Am. Chem. Soc.* **2002**, *124*, 9042.
(20) (a) Yamamoto, T.; Arif, A. M.; Stang, P. J. *J. Am. Chem. Soc.* **2003**, *125*, 12309. (b) Diaz, P.; Torilla, J. A.; Ballester, P.; Benet-Buchholz, J.; Vilar, R. *J. Chem. Soc., Dalton Trans.* **2007**, 3516. (c) Bark, T.; Düggeli, M.; Stoeckli-Evans, H.; von Zelewsky, A. *Angew. Chem., Int. Ed.* **2001**, *40*, 2848.
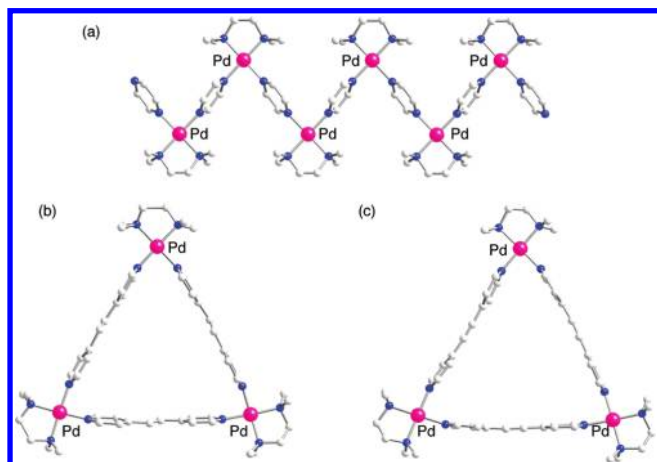(21) Jiang, H.; Lin, W. *J. Am. Chem. Soc.* **2006**, *128*, 11286.
(22) Jones, P. L.; Byrom, K. J.; Jeffery, J. C.; McCleverty, J. A.; Ward, M. D. *J. Chem. Soc., Chem. Commun.* **1997**, 1361.
(23) (a) Weilandt, T.; Troff, R. W.; Saxell, H.; Rissanen, K.; Schalley, C. A. *Inorg. Chem.* **2008**, *47*, 7588. (b) Schalley, C. A.; Müller, T.; Linnartz, P.; Witt, M.; Schäfer, M.; Lützen, A. *Chem.—Eur. J.* **2002**, *8*, 3538.
(24) Holló-Sitkei, E.; Tárkányi, G.; Párkányi, L.; Lárkányui, L.; Megyes, T.; Besenyei, G. *Eur. J. Inorg. Chem.* **2008**, 1574.
(25) (a) Chun, I. S.; Moon, S. J.; Na, Y. M.; Lee, Y.-A.; Yoo, K. H.; Jung, O.-S. *Inorg. Chem. Commun.* **2007**, *10*, 967. (b) Noh, T. H.; Moon, S. J.; Na, Y. M.; Ha, B. J.; Jung, O.-S. *Inorg. Chem. Commun.* **2008**, *11*, 1334.

Results and Discussion

Syntheses and Characterizations of Solid Molecular Triangles $[(en^*)Pd(L_n)]_3(NO_3)_6$ na·NO$_3$ (n = 3, 4) and an Infinite Chain Complex 1 with the L$_1$ Ligand. To clarify

Figure 1. Molecular structures of (a) **1**, (b) **3a·NO₃**, and (c) **4a·NO₃**. Nitrate anions are omitted for clarity.

effects of the bridging and supporting ligands on the resultant supramolecular structures, Pd-based compounds with a series of the bridging ligands of L_1 and $L_3–L_5$ were synthesized. The reactions of (en*)Pd(NO₃)₂ with the bridging ligands in H_2O gave the yellow precipitates, and the recrystallization by vapor diffusion of acetone into dimethylsulfoxide (DMSO) yielded the pale yellow crystalline solids in moderate to high yields (50−97%, Supporting Information, Table S1). The IR spectra showed the bands of the C−H (2909−3088 cm⁻¹), C=N (1612−1613 cm⁻¹), and N−O (1384 cm⁻¹) stretching vibrations (Supporting Information, Figures S1 and S2), suggesting the complexation of (en*)Pd(NO₃)₂ with the corresponding bridging ligands. The elemental analyses also suggest the formation of $\{[(en*)Pd(L_n)](NO_3)_2\}_m$ with the (en*)Pd²⁺/L_n ratio 1:1.

The solid molecular triangles $[(en*)Pd(L_n)]_3(NO_3)_6$ ($n = 3$ (**3a·NO₃**), 4 (**4a·NO₃**)) could successfully be characterized by the X-ray crystallography (Figure 1 and Tables 1 and 2).

Table 1. Crystallographic Data for **1**, **3a·NO₃**, and **4a·NO₃**

	1	**3a·NO₃**	**4a·NO₃**
empirical formula	C₄₀N₂₀O₁₂Pd₄	C₅₄N₁₈O₁₈Pd₃	C₅₈H₇₂N₁₈O₂₀Pd₃S₂
formula weight	1378.2	1507.92	1724.66
crystal system	monoclinic	monoclinic	orthorhombic
lattice type	*primitive*	*primitive*	*C*-centered
space group	$P2_1/m$ (No. 11)	Pn (No. 7)	$Aba2$ (No. 41)
lattice parameter	$a = 14.4740(7)$ Å	$a = 17.3242(3)$ Å	$a = 14.6642(3)$ Å
	$b = 8.9209(3)$ Å	$b = 15.0804(3)$ Å	$b = 27.8763(5)$ Å
	$c = 28.9705(13)$ Å	$c = 17.3223(3)$ Å	$c = 21.4233(4)$ Å
	$\beta = 89.974(2)°$	$\beta = 103.5100(10)°$	
	$V = 3740.7(3)$ Å³	$V = 4400.33(14)$ Å³	$V = 8757.5(3)$ Å³
Z	2	2	4
d_{calcd}	1.224 g cm⁻³	1.138 g cm⁻³	1.308 g cm⁻³
μ(Mo K$_\alpha$)	9.99 cm⁻¹	6.65 cm⁻¹	7.24 cm⁻¹
no. of reflection measured	10860	12165	6281
no. of observations[a]	5024	9274	5652
no. of variables	303	642	376
R	0.0888	0.0848	0.0645
wR_2	0.2719	0.2382	0.1859

[a] Data with $I > 2.0\sigma(I_o)$.

Table 2. Selected Bond Lengths and Angles for **1**, **3a·NO₃**, and **4a·NO₃**[a]

compound	**1**[b,c] molecule A	molecule B	**3a·NO₃**	**4a·NO₃**[b]
Pd−N(en*)	2.037(7), 2.082(6)	2.045(7), 2.088(6)	2.107(10), 2.090(8) 2.059(9), 2.083(9) 2.079(7), 2.063(7)	2.046(13), 2.037(15)
Pd−N(Py)	2.033(3), 2.048(6)	2.032(3), 2.047(3)	2.031(5), 2.023(5) 2.044(5), 2.033(4) 2.020(8), 2.041(7)	2.022(12), 2.017(12)
Pd···Pd	6.8522(15)	6.8518(15)	13.382(7), 13.297(6) 13.296(6)	13.517(13), 13.654(18)
N(en*)-Pd−N(en*)	82.8(5), 87.6(3)	86.0(4), 85.1(4)	86.1(5), 87.4(5) 86.3(3)	86.1(7), 85.7(9)
N(en*)−Pd−N(Py)	95.7(3), 92.7(3)	94.3(2), 93.9(2)	93.3(3), 94.6(4) 94.1(4), 93.6(4)	93.0(5), 93.5(5)
N(Py)−Pd−N(Py)	85.8(3), 87.1(4)	85.5(3), 86.9(4)	86.0(3), 84.9(3) 83.4(6)	87.9(7), 87.0(7)
torsion angle (Py··Py plane)			13.43, 2.36 0.80	17.17, 3.34

[a] Distances in angstrom and angles in degree. [b] Sitting on a crystallographical mirror plane. [c] Molecules A and B are crystallographically independent.

The ethylene double bond in L_3 and acetylene triple bond in L_4 were retained in $\mathbf{3a \cdot NO_3}$ and $\mathbf{4a \cdot NO_3}$, respectively. The Pd$\cdots$Pd distances (13.296−13.383 Å) in $\mathbf{3a \cdot NO_3}$ were similar to the Pt$\cdots$Pt distances (13.315−13.548 Å) in $[(Me_3P)_2Pt(L_3)]_3(X)_6$, (X = OTf$^-$, CoB$_{18}C_4H_{22}^-$)[5b] and $[(dppp)Pt(L_3)]_3(OTf)_6$.[14] The Pd$\cdots$Pd distances of $\mathbf{4a \cdot NO_3}$ were 13.517−13.654 Å and a little longer than those in $\mathbf{3a \cdot NO_3}$. The nitrate anions in $\mathbf{3a \cdot NO_3}$ and $\mathbf{4a \cdot NO_3}$ existed at the axial positions of the cationic Pd(II) centers and compensated the cationic charges. The N(Py)−Pd−N(Py) angles in $\mathbf{na \cdot NO_3}$ (n = 2−4) were 82.4(4)°−86.0(4)°, 83.4(6)°−86.0(3)°, and 87.0(7)°−87.9(7)°, respectively, and increased closely to 90° with the increase in the lengths of the bridging ligands, indicating the relaxation of the steric hindrance from $\mathbf{2a \cdot NO_3}$ to $\mathbf{4a \cdot NO_3}$ since a 90° angle has been observed for the ideal square planar Pd(II) complexes.

On the other hand, a solid infinite chain compound $\{[(en^*)Pd(L_1)](NO_3)_2\}_\infty$ **1** was formed upon the use of the shortest L_1 bridging ligand (Figure 1a).[26] The N(Py)−Pd−N(Py) angles were 85.5(3)°−87.1(4)° and larger than those (82.4(4)−86.0(4)°) in $\mathbf{2a \cdot NO_3}$. The steric effects between the supporting and the bridging ligands on the formation of molecular triangles and squares have also been proposed by Alessio et al. and Besenyei et al.[12,24] Molecular triangles of $[(Me_3P)_2Pt(L_1)]_3(OTf)_6$ and [$trans,cis$-RuCl$_2$(DMSO-S)$_2$(L$_1$)]$_3$ are formed upon the use of the bulky trimethylphosphine and DMSO supporting ligands,[5a,12] while molecular squares of $[(en)Pt(L_1)]_4(NO_3)_8$ and $[(H_3N)_2Pt(L_1)]_4$-$(NO_3)_8$ are formed upon the use of the less bulky ethylenediamine and ammonia supporting ligands.[7b,16i] A molecular triangle, $[(en^*)Pd(L)]_3(PF_6)_3$ (L = nicotinate), and the corresponding trimeric chain complex have been reported by Jung et al. upon the use of bulky en* as a supporting ligand.[25] Therefore, the infinite chain complex of **1** would be formed to avoid the increase in the steric hindrance between the supporting and the shortest bridging ligands or neighboring supporting ligands.[27−29]

(26) The ^{1}H NMR spectrum of **1** in D$_2$O at 298 K showed the two sets of the signals of L$_1$ ligand with the intensity ratio 0.94:1.16:1.16:0.94. At 353 K, the two sets of signals coalesced into the two broad singlet signals at 9.62 and 9.44 ppm with the intensity ratio 1.00:1.00. These facts show the fractional behavior of the rotation of the supporting or bridging ligand in the solution state. Therefore, the dissolved species of **1** is not an infinite chain complex, but a monomeric [(en*)Pd(L$_1$)(solvent)](NO$_3$)$_2$.

(27) Fujita et al. have reported the formation of the oligomeric species upon the dissolution of [(en)Pd(L$_4$)]$_4$(NO$_3$)$_8$ in water at the high concentration.

(28) We have also reported the formation of an infinite chain complex of $\{[(en)Pd(L_1)]_2[\alpha$-SiW$_{12}$O$_{40}]\}_\infty$ in the presence of the bulky counter anion: Uehara, K.; Nakao, H.; Kawamoto, R.; Mizuno, N. *Inorg. Chem.* **2006**, *45*, 9448.

(29) The platinum complex [(Me$_3$P)$_2$Pt(L$_1$)]$_3$(OTf)$_6$ with the more sterically hindered PMe$_3$ ligand forms the triangular complex. The trans effect of the phosphine ligand would render the Pt−N(L$_1$) distances (2.11(2)−(2.14(2)Å) longer than the Pd−N(L$_1$) distances of Pd infinite complex **1** (2.032(3)−2.047(3)Å), resulting in the relaxation of the steric repulsion between the neighboring supporting ligands of [(Me$_3$P)$_2$Pt(L$_1$)]$_3$(OTf)$_6$.

(30) The ^{1}H NMR spectrum upon the dissolution of $\mathbf{3a \cdot NO_3}$ exhibited the vinyl proton signal at 7.60 ppm. The ^{13}C{H}NMR spectra of $\mathbf{3a \cdot NO_3}$ and $\mathbf{3b \cdot NO_3}$ and those of $\mathbf{4a \cdot NO_3}$ and $\mathbf{4b \cdot NO_3}$ also showed the C=C and C≡C signals at 151.25 and 92.24 ppm, respectively, while the IR bands of the corresponding stretching vibrations were not observed. The disappearance of the IR bands is probably explained by the very weak intensities in highly symmetric structures of **na** and **nb** obtained with the DFT frequency calculations.

Equilibrium between Molecular Triangles and Squares. First, the ^{1}H NMR spectra were measured upon the dissolution of $\mathbf{na \cdot NO_3}$ (n = 2−5) and $\mathbf{2'b \cdot NO_3}$ at various concentrations to assign the signals of $\mathbf{na \cdot NO_3}$ and $\mathbf{nb \cdot NO_3}$ (Supporting Information, Table S1).[30] The molecular square was observed upon the dissolution of $\mathbf{2'b \cdot NO_3}$ in DMSO-d_6. It has also been reported by Fujita et al. that only the molecular square was observed (α = 1.000) upon the dissolution of $\mathbf{2'b \cdot NO_3}$ in D$_2$O.[4a] On the other hand, two sets of the signals derived from the bridging and supporting ligands were observed upon the dissolution of $\mathbf{na \cdot NO_3}$ (n = 2−4) and $\mathbf{5 \cdot NO_3}$ in DMSO-d_6, indicating the equilibrium between the molecular triangles and the squares (Supporting Information, Figures S4−S7). These facts show that the introduction of methyl substituents into the en supporting ligand (en*) induces the equilibrium. The destabilizing effect of bulky supporting ligands has been reported by Fujita et al.[4a] The signals of the methyl substituents of en* in $\mathbf{na \cdot NO_3}$ (n = 2−5) were observed in the lower magnetic fields (2.59−2.61 ppm) than those in $\mathbf{nb \cdot NO_3}$ (2.45 ppm), showing that the methyl and pyridyl moieties in $\mathbf{na \cdot NO_3}$ are less sterically hindered than those in the corresponding $\mathbf{nb \cdot NO_3}$.
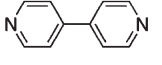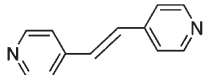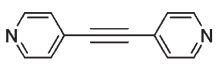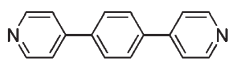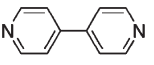
The $Py(\alpha)$ signals of $\mathbf{na \cdot NO_3}$ (n = 3−5) were observed at 9.03, 9.14, and 9.14 ppm, respectively, while those of the corresponding $\mathbf{nb \cdot NO_3}$ (n = 3−5) were observed at 9.14, 9.22, and 9.23 ppm, respectively. The appearances of the $Py(\alpha)$ signals of $\mathbf{na \cdot NO_3}$ in the higher magnetic fields than those of the corresponding $\mathbf{nb \cdot NO_3}$ in accord with the appearance of the signals of the methyl substituents of $\mathbf{na \cdot NO_3}$ in the lower magnetic fields, and probably results from the stronger interactions of the pyridyl rings coordinated to the same Pd center of the molecular triangles.[11] Thus, the steric hindrance between the *cis*-coordinated pyridyl moieties influences the chemical shifts of $Py(\alpha)$ signals of the bridging ligands. On the other hand, the $Py(\beta)$ signals of $\mathbf{na \cdot NO_3}$ (n = 3−5) were observed at 7.68, 7.75, and 8.08 ppm, respectively, while those of the corresponding $\mathbf{nb \cdot NO_3}$ (n = 3−5) were observed at 7.80, 7.81, and 8.16 ppm, respectively. Therefore, the $Py(\beta)$ signals of $\mathbf{na \cdot NO_3}$ appeared in the higher magnetic fields than those of the corresponding $\mathbf{nb \cdot NO_3}$ in the same manner as that of the $Py(\alpha)$ signals.

We have reported that the $Py(\alpha)$ and $Py(\beta)$ signals of $\mathbf{2a \cdot NO_3}$ appeared at 9.18 and 8.14 ppm, respectively, and those of $\mathbf{2b \cdot NO_3}$ appeared at 9.32 and 8.12 ppm, respectively. The $Py(\alpha)$ signal of $\mathbf{2a \cdot NO_3}$ appeared in the higher magnetic field than that of $\mathbf{2b \cdot NO_3}$ in the same manner as those for $\mathbf{na \cdot NO_3}$ and $\mathbf{nb \cdot NO_3}$ (n = 3−5). In contrast, the $Py(\beta)$ signal of $\mathbf{2a \cdot NO_3}$ appeared in the lower magnetic field than that of $\mathbf{2b \cdot NO_3}$. This higher magnetic field shift is probably because $\mathbf{2b \cdot NO_3}$ is more strained by the twisting of the pyridyl rings (21.89° and 32.02°) than $\mathbf{2a \cdot NO_3}$ (16.36°−20.87°).

The degrees of dissociations (α) changed with the lengths of the bridging ligands in DMSO-d_6 and increased in the order of $\mathbf{3 \cdot NO_3}$ < $\mathbf{2 \cdot NO_3}$ < $\mathbf{4 \cdot NO_3}$ < $\mathbf{5 \cdot NO_3}$ (Table 3).[31] The $\Delta G°$ values decreased in the reverse order of $\mathbf{3 \cdot NO_3}$ > $\mathbf{2 \cdot NO_3}$ > $\mathbf{4 \cdot NO_3}$ > $\mathbf{5 \cdot NO_3}$. The decrease in

(31) The α values for $\mathbf{4a \cdot NO_3}$ and $\mathbf{5a \cdot NO_3}$ could be obtained only in DMSO, because $\mathbf{4a \cdot NO_3}$ and $\mathbf{5a \cdot NO_3}$ were insoluble in the other solvents.

Table 3. Experimental Data for Equilibrium in Solvents

Equilibrium[a]	Supporting ligand	Bridging ligand (N···N length (Å))	Solvent	C^b (mM)	$K_{eq}{}^c$ (M^{-1})	Exp.	
						α^d	$\Delta G°$ (kJ mol^{-1})^e
2·NO₃	en*	N—⬡—⬡—N (7.061)	DMSO-d_6	9.72	5.38	0.310	−4.17
			D₂O	9.28	1.36×10^3	0.680	−11.9
			DMF-d_7	10.3	0.978	0.210	0.0532
3·NO₃	en*	(9.408)	DMSO-d_6	10.2	0.852	0.203	0.373
			D₂O	10.0	0.019	0.070	9.575
4·NO₃	en*	(9.593)	DMSO-d_6	12.4	19.6	0.411	−7.37
5·NO₃	en*	(11.40)	DMSO-d_6	9.98	40.9	0.609	−9.00
2'·NO₃^f	en	(7.061)	DMSO-d_6	10.0	–	1.000	–
			D₂O	10.0	–	1.000	–

^{a} **n·NO₃** shows the equilibrium between **na·NO₃** and **nb·NO₃** according to eq 1. ^{b} Concentration as a molecular triangle. The diluted solutions were used to ignore the ionic strengths and related activity constants. ^{c} Equilibrium constant: $K_{eq} = 27\alpha^3/64C(1-\alpha)^4$. ^{d} The α values were calculated according to the equation of $K_{eq} = \exp(-\Delta G°/RT)$. ^{e} The $\Delta G°$ values were estimated according to the equation of $\Delta G° = -RT \ln K_{eq}$ ($R = 8.314$ J mol^{-1} K^{-1}, $T = 298.15$ K). ^{f} Synthesized according to ref 4a.

the $\Delta G°$ values in the order of **2·NO₃** > **4·NO₃** > **5·NO₃** suggests that the molecular squares are more stabilized than the corresponding molecular triangles with the increase in the lengths of the straight bridging ligands. While the L₃ length (9.362(41) Å) was comparable to that of L₄ (9.594(2) Å), the $\Delta G°$ value for **3·NO₃** was larger than that of **4·NO₃**. This is probably because the angular L₃ ligand stabilizes the molecular triangle more than the corresponding molecular square. A similar stabilization of molecular triangles with angular pyrimidine and bipyrimidine bridging ligands has been reported for triangle Pt(II) complexes by Che et al.[6] and Lippert et al.[7a]

Upon the dissolution of **2a·NO₃** in the solvents, the ¹H NMR spectra showed that the α values decreased in the order of DMF > DMSO > H₂O. Thus, the equilibrium between the molecular triangle and square also depends on the kinds of the solvents. The importance of the solvent in the equilibrium has also been proposed by Schalley et al.[23a]
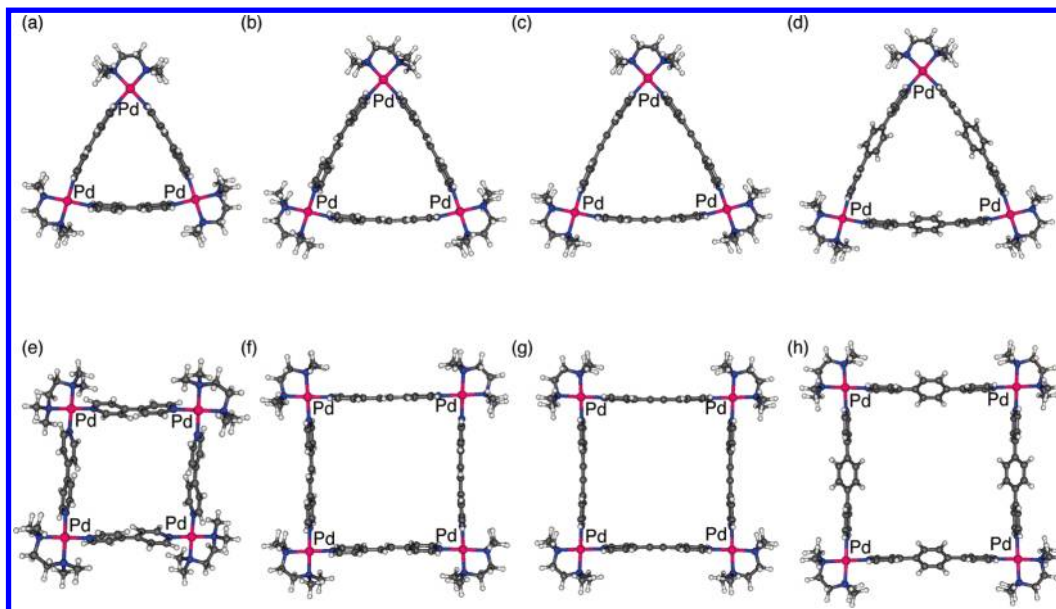
Investigation of the Equilibrium between Molecular Triangles and Squares with DFT Calculations in the Solutions. First, the structures of the cationic moieties of the molecular triangles **na** and squares **nb**, [(en*)Pd(L$_n$)]$_m^{2m+}$ ($n=2-5$) and [(en)Pd(L$_n$)]$_m^{2m+}$ ($n=2'$), under the vacuum conditions were optimized with the DFT calculations. The calculated $\Delta G°$ values were $1.59 \times 10^3 - 1.90 \times 10^3$ kJ mol^{-1} (Supporting Information, Table S5), and quite different from experimental data, suggesting that the presence of solvents can not be ignored. Therefore, the

structures of the cationic molecular triangles and squares in solutions were investigated with the DFT calculation using the conductor-like polarizable continuum model (C-PCM), and only the optimization of **na** and **nb** in water was successful.[32] The calculated structural parameters such as Pd−N(en*), Pd−N(Py), and Pd···Pd distances around the palladium metal centers are shown in Supporting Information, Tables S3 and S4, and Figure 2. These structural parameters of **2a−4a** and **2b** in water better reproduced the respective experimental data in the solid states than those calculated under the vacuum conditions.[33] Therefore, the structures of **na** and **nb** optimized in water were used for the calculations of the $\Delta G°$ values in the solvents.

In the single-point energy C-PCM calculation, $\Delta G°$ can be expressed by eq 2, where ΔG(vac), ΔE(es), and ΔE(nes) are the changes in the Gibbs-free energy of the supramolecular frameworks under the vacuum conditions,

(32) It was confirmed that the structures of **4a** and **4b** optimized in DMSO were similar to those of **4a** and **4b** optimized in water.

(33) The ¹H NMR spectra of **na** and **nb** ($n=2-5$) in DMSO were estimated with the GIAO-DFT calculations. The calculated signal positions were very close to those obtained experimentally (Supporting Information, Table S6) and well reproduced the experimental trends: (i) The signals of the methyl substituents of the en* supporting ligands in **na** ($n=2-5$) were calculated to appear in the lower magnetic fields than those in **nb**, (ii) the $Py(\alpha)$ and $Py(\beta)$ signals of **na** ($n=3-5$) were calculated to appear in the higher magnetic field than those in **nb** ($n=3-5$), (iii) the $Py(\alpha)$ signal of **2a** was calculated to appear in the higher magnetic fields than that of **2b**, whereas the $Py(\beta)$ signal of **2a** was calculated to appear in the lower magnetic field than that in **2b**.

Figure 2. Structures of cationic parts of **na** and **nb** ($n = 2-5$) optimized in water. (a)−(d) are **2a**−**5a**, respectively, and (e)−(h) are **2b**−**5b**, respectively. [34]

Table 4. Calculated ΔG(vac), ΔE(es), and $\Delta G°$ Values for Equilibrium in Solvents

equilibrium[a]	solvent	ΔG(vac) (kJ mol^{-1})	ΔE(es) (kJ mol^{-1})	ΔE(nes) (kJ mol^{-1})	$\Delta G°$ (kJ mol^{-1})
2	DMSO	2.002×10^3	-2.060×10^3	52.51	−5.77
	H$_2$O	2.002×10^3	-2.066×10^3	51.76	−12.34
	DMF	2.002×10^3	-2.045×10^3	69.96	26.28
3	DMSO	1.638×10^3	-1.622×10^3	8.74	26.27
4	DMSO	1.611×10^3	-1.610×10^3	−14.90	−13.65
5	DMSO	1.415×10^3	-1.415×10^3	−17.87	−25.89
2′	DMSO	1.979×10^3	-1.994×10^3	−8.08	−23.10
	H$_2$O	1.979×10^3	-2.007×10^3	−7.57	−35.53

^{a} **n** shows the equilibrium between **na** and **nb** according to eq 1.

the electrostatic energy by the ion-dipole interaction between the cationic supramolecule and solvent, and the non-electrostatic energy by the repulsion between the supramolecular framework and solvent, respectively. The calculation results are summarized in Table 4.

$$\Delta G° = \Delta G(\text{vac}) + \Delta E(\text{es}) + \Delta E(\text{nes}) \qquad (2)$$

The effect of the supporting ligand on the equilibrium was investigated. The $\Delta G°$ values for **2′** calculated in DMSO and H$_2$O were −28.84 and −35.33 kJ mol^{-1}, respectively, and much negative, in fair agreement with the fact that only the molecular square of **2′b** was observed in DMSO and D$_2$O. On the other hand, the $\Delta G°$ values for **2** calculated in DMSO and H$_2$O were −5.72 and −12.16 kJ mol^{-1}, respectively, in agreement with the presence of the equilibrium of **2**, and much larger than those for **2′**. Thus, the effect of the introduction of the methyl substituents into the en supporting ligand was reproduced by the calculation.

Next, the effect of the supramolecular sizes with the straight bridging ligands on the equilibrium of **2**, **4**, and **5** was investigated. The ΔG(vac) values decreased with the increase in the supramolecular sizes in the order of **2** (2.002×10^3 kJ mol^{-1}) > **4** (1.611×10^3 kJ mol^{-1}) > **5** (1.415×10^3 kJ mol^{-1}). On the other hand, the ΔE(es) values increased with the increase in the supramolecular sizes in the order of **2** (-2.060×10^3 kJ mol^{-1}) < **4**

(-1.610×10^3 kJ mol^{-1}) < **5** (-1.415×10^3 kJ mol^{-1}), and approximately compensated the corresponding ΔG-(vac) values. The ΔE(nes) values decreased with the increase in the lengths of the bridging ligands in the order of **2** (52.51 kJ mol^{-1}) > **4** (−14.90 kJ mol^{-1}) > **5** (−17.50 kJ mol^{-1}).[35] Consequently, the $\Delta G°$ values decreased with the increase in the supramolecular sizes in the same order of **2** (−5.77 kJ mol^{-1}) > **4** (−13.65 kJ mol^{-1}) > **5** (−25.89 kJ mol^{-1}) as that of ΔE(nes).[36,37]

(34) Molekel 5.3, the molecular visualization program developed by the Visualization Group at the Swiss National Supercomputing Center (CSCS).

(35) The ΔG(vac) and ΔE(es) values for **3** with an angular bridging ligand of L$_3$ were calculated to be 1.638×10^3 kJ mol^{-1} and -1.622×10^3 kJ mol^{-1}, respectively. The respective values were close to those of **4** (1.611×10^3 kJ mol^{-1} and -1.610×10^3 kJ mol^{-1}). On the other hand, the ΔE(nes) value for **3** was calculated to be 8.74 kJ mol^{-1}, which was much larger than that for **4** (−14.90 kJ mol^{-1}), although the length of the bridging ligand (9.593 Å) was close to that of L$_3$ (9.408 Å). This is probably because of the more significant steric repulsion between the hindered molecular square **3b** and the solvents than that of **4a**. Therefore, the $\Delta G°$ value (26.27 kJ mol^{-1}) for **3** was the highest among those systems.

(36) The change in the ΔE(nes) values is possibly explained by the increase in the relaxation of the steric repulsion between the supramolecular frameworks and solvents with the increase in the sizes of the supramolecular frameworks.

(37) The void volumes increased in the order of **2a** (651 Å) < **4a** (1035 Å) < **5a** (1512 Å) and **2b** (1118 Å) < **4b** (2186 Å) < **5b** (2954 Å), and the change in the void volumes according to eq. 1 increased in the order of **2** (467 Å^3) < **4** (1151 Å^3) < **5** (1442 Å^3). The change would be related to the stabilization of the frameworks by the encapsulation of the solvents, leading to the reverse order of the $\Delta G°$ values.

Finally, the effect of DMSO, H_2O, and N,N-dimethylformamide (DMF) solvents on the equilibrium was investigated. The $\Delta G(\text{vac})$ value was 2.002×10^3 kJ mol^{-1}, which was independent of the kinds of the solvents. The $\Delta E(\text{es})$ values approximately compensated the $\Delta G(\text{vac})$ values, while the $\Delta E(\text{es})$ values slightly decreased in the order of DMF (-2.045×10^3 kJ mol^{-1}) > DMSO (-2.060×10^3 kJ mol^{-1}) > H_2O (-2.066×10^3 kJ mol^{-1}) and in the reverse order of the relative permittivity (DMF (36.71) < DMSO (46.70) < H_2O (78.39)). The $\Delta E(\text{nes})$ values decreased in the order of DMF (69.96 kJ mol^{-1}) > DMSO (52.51 kJ mol^{-1}) > H_2O (51.76 kJ mol^{-1}). The order was the same as that of the solvent sizes (DMF (radius = 2.647 Å) > DMSO (2.455 Å) > H_2O (1.385 Å)) probably because of the decrease in the steric repulsion between the supramolecules and solvents with the decrease in the solvent sizes. Consequently, the $\Delta G°$ values decreased in the same order of DMF (26.28 kJ mol^{-1}) > DMSO (-5.77 kJ mol^{-1}) > H_2O (-12.34 kJ mol^{-1}) as that of $\Delta E(\text{nes})$. Thus, the effects of the straight bridging ligands and solvents on the equilibrium were well reproduced by the calculated data.

Conclusion

The factors controlling the structures of the molecular triangles and squares and the equilibrium were studied. Larger molecular triangles [(en*)Pd(L$_3$)]$_3$(NO$_3$)$_6$ **3a·NO$_3$** and [(en*)Pd(L$_4$)]$_3$(NO$_3$)$_6$ **4a·NO$_3$** and an infinite chain compound [(en*)Pd(L$_1$)(NO$_3$)$_2$]$_\infty$ **1** could be synthesized and fully characterized. The X-ray crystallography and ^{1}H NMR spectroscopy indicated that the steric hindrance between the supporting and the bridging ligands or the neighboring supporting ligands and the lengths and shapes of the bridging ligands would contribute to the structures of the supramolecules in the solid states and the equilibrium between the molecular triangle and square in the solutions. The DFT calculations of the cationic moieties of the molecular triangles **na** and squares **nb** ($n = 2-5$, 2′) using the conductor-like polarizable continuum model could reproduce the following experimental results (i)−(iii): (i) the equilibrium between the molecular triangles and the squares was attained upon the introduction of the methyl substituents into the en supporting ligands (en*), (ii) the $\Delta G°$ values decreased with the increase in the lengths of the straight bridging ligands, and (iii) the equilibrium constants depended on the kinds of solvents.

Experimental Section

General Procedures. All manipulations except for the ligand syntheses were carried out under the aerobic conditions. The palladium complex (en*)PdCl$_2$,[38] 1,2-bis(4-pyridyl)acetylene (L$_4$),[39] and 1,4-bis(4-pyridyl)benzene (L$_5$)[40] were synthesized according to the literature. The other reagents were used as purchased. The syntheses of **2a·NO$_3$** and **2b·NO$_3$** were carried out according to our previous report.[13] The ^{1}H (270 MHz) and ^{13}C{H} (67.8 MHz) NMR spectra were recorded on JEOL EX-270 equipped with Excalibur 6.0 for Windows. Infrared spectra were recorded on JASCO FT-IR 580.

Diffraction measurements were made on a Rigaku Micro-Max-007 with Mo Kα radiation ($\lambda = 0.71069$ Å). The data collections were carried out at 153 K. Indexing was performed from 12 oscillation images, which were exposed for 5 s. The crystal-to-detector distance was 45 mm. Readout was performed with the pixel size of 72.4 × 72.4 mm. A sweep of data was done using ω scans from $-110°$ to 70° at $\kappa = 45°$ and $\phi = 0°$, 90°. A total of 720 images for each compound were collected. Neutral scattering factors were obtained from the standard source.[41] Data were corrected for Lorentz and polarization effects. Empirical absorption corrections were made with HKL 2000 for Linux.[42] Molecular structures were solved by SHELX-97[43] linked to Win-GX for Windows.[44]

The details of X-ray crystallography for each compound are mentioned in the Supporting Information. CCDC 745210 (**1**), 745211 (**3a·NO$_3$**), and 745212 (**4a·NO$_3$**) contain the supplementary crystallographic data. The data can be obtained free of charge via www.ccdc.cam.ac.uk/conts/retrieving.html (or from the Cambridge Crystallographic Data Centre, 12, Union Road, Cambridge CB2 1EZ, U.K.; Fax: (+44) 1223−336−033; or deposit@ccdc.cam.ac.uk).

Synthesis of [(en*)Pd(L$_1$)(NO$_3$)$_2$]$_\infty$ (1). The reaction of (en*)PdCl$_2$ (0.300 g, 1.02 mmol) with 2 equiv of AgNO$_3$ (0.347 g, 2.04 mmol) in 20 mL of H_2O led to the immediate formation of the AgCl precipitate. After stirring for 2 h, the AgCl precipitate was filtrated. Addition of pyrazine (L$_1$) (0.0819 g, 1.02 mmol) to the filtrate and stirring overnight gave the yellow solution. After concentration of the solution, addition of acetone into the solution gave the pale-yellow precipitate. The recrystallization from acetone/H_2O gave the single crystal of **1** (0.283 g, 0.662 mmol, 64.9% yield). IR(KBr, cm^{-1}) 3019 w, 2984 w, 2906 w, 2841 w (ν_{C-H}), 1763 w, 1640 m, 1467 m, 1416 m ($\nu_{C=C}$), 1384 vs (ν_{N-O}), 1239 w, 1207 w, 1123 w, 1103 w, 1063 w, 1046 w, 1030 w, 1006 w, 953 w, 825 w, 805 m, 765 w, 500 w, 416 w, 254 vs ^{1}H NMR (270 MHz, D$_2$O, 298 K) δ_H (ppm), 9.41 (d, $^2J = 3.24$ Hz, L$_1$), 9.11 (d, $^2J = 3.24$ Hz, L$_1$), 8.92 (d, $^2J = 3.24$ Hz, L$_1$), 8.84 (d, $^2J = 3.24$ Hz, L$_1$), 3.13−2.88 (m, CH_2), 2.75 (s, Me), 2.67 (s, Me), 2.64 (s, Me). (353 K) 9.62 (brs, 2H, L$_1$), 9.44 (brs, 2H, L$_1$), 3.45 (brs, CH_2, 4H), 3.20 (s, 12H, Me). ^{13}C{H}NMR (67.8 MHz, D$_2$O, 353 K) δ_C (ppm) 122.17, 121.65, 120.15, 119.41 (L$_1$), 37.68, 36.57, 35.40 (CH_2), 24.69, 24.02, 23.13 (Me). Anal. Calcd for C$_{10}$PdH$_{22}$O$_7$N$_6$ (**1·H$_2$O**): C, 27.01; H, 4.99; N, 18.90%. Found: C, 26.61; H, 4.97; N, 18.89%.

Synthesis of [(en*)Pd(L$_3$)]$_m$(NO$_3$)$_{2m}$ (3a·NO$_3$ ($m = 3$), 3b·NO$_3$ ($m = 4$)). The reaction of (en*)PdCl$_2$ (0.300 g, 1.02 mmol) with 2 equiv of AgNO$_3$ (0.347 g, 2.04 mmol) in 20 mL of H_2O led to the immediate formation of the AgCl precipitate. After stirring for 2 h, the AgCl precipitate was filtrated. Addition of 1,2-bis(4-pyridyl)ethylene (L$_3$) (0.347 g, 1.02 mmol) to the filtrate and stirring overnight gave the white-yellow emulsion. After removal of volatiles, the resultant solid was dissolved in 2 mL of DMSO. The remaining AgCl was removed from the solution by centrifugation, and the resulting solution was filtered. The recrystallization from DMSO/acetone gave the single crystal of **3a·NO$_3$** (0.525 g, 0.331 mmol, 97% yield). IR(KBr, cm^{-1}) 3085 w, 3006 w 2920 w (ν_{C-H}), 1612 ($\nu_{C=N}$), 1509 w, 1473 w, 1438 m 1384 vs (ν_{N-O}), 1211 m, 1128 w, 1074 w, 1025 m, 957 w, 844 m, 812 m, 772 w, 584 m, 558 m. ^{1}H NMR (270 MHz, DMSO-d_6) δ_H (ppm) 9.14 (d, $^2J = 6.48$ Hz, Py (**3b·NO$_3$**)), 9.03 (d, $^2J = 6.48$ Hz, Py (**3a·NO$_3$**)), 7.80 (d, $^2J = 6.48$ Hz,

(38) (a) Wojciechowski, W.; Matczak-jon, E. *Inorg. Chim. Acta* **1990**, *173*, 85. (b) Djuran, M. I.; Milinkovic, S. U. *Polyhedron* **2000**, *19*, 959.

(39) (a) Yu, L.; Lindsey, J. S. *J. Org. Chem.* **2001**, *66*, 7402. (b) Ribou, A.-C.; Wada, T.; Sasabe, H. *Inorg. Chim. Acta* **1999**, *288*, 134.

(40) Biradha, K.; Hongo, Y.; Fujita, M. *Angew. Chem., Int. Ed.* **2000**, *39*, 3843.

(41) *International Tables for X-ray Crystallography*; Kynoch Press: Birmingham, U.K., 1975; Vol. *4*.

(42) Otwinowski, Z.; Minor, W. In *Processing of X-ray Diffraction Data Collected in Oscillation Mode, Methods in Enzimology, Macromolecular Crystallography, Part A*; Carter, C. W., Jr., Sweet, R. M., Eds.; Academic Press: New York, 1997; Vol. *276*, p 307.

(43) Sheldrick, G. M. *SHELX-97, Programs for Crystal Structure Analysis*, release 97-2; University of Göttingen: Göttingen, Germany, 1997.

(44) Farrugia, L. J. *J. Appl. Crystallogr.* **1999**, *32*, 837.

Py (**3b·NO₃**)), 7.68 (d, $^2J = 6.48$ Hz, *Py* (**3a·NO₃**)), 7.60 (s, =*CH* (**3b·NO₃**)), 7.51 (s, =*CH* (**3a·NO₃**)), 2.96 (brs, *CH₂*), 2.60 (brs, *Me*). ^{13}C{H}NMR (67.8 MHz, DMSO-d_6, ppm) δ_C 151.25 (=*CH*), 146.26 (*Py*(α), **3b·NO₃**), 145.96 (*Py*(α), **3a·NO₃**), 131.99 (*Py*(ipso), **3b·NO₃**), 131.85 (*Py*(ipso), 124.55 (*Py*(β), 3a·NO₃), 124.55 (*Py*(β), **3b·NO₃**), 124.15 (*Py*(β), **3a·NO₃**), 62.17 (*CH₂*), 50.27 (*Me*). Anal. Calcd for $C_{82}Pd_4S_5H_{146}O_{35}N_{24}$ (**3a·NO₃·5DMSO·6H₂O**): C, 37.67; H, 5.63; N, 12.86; S, 6.13%. Found: C, 37.34; H, 5.90; N, 12.63; S, 5.86%.

Synthesis of [(en*)Pd(L₄)]$_m$(NO₃)$_{2m}$ (4a·NO₃ (m = 3), 4b·NO₃ (m = 4)). The reaction of (en*)PdCl₂ (0.305 g, 1.04 mmol) with 2 equiv of AgNO₃ (0.347 g, 2.04 mmol) in 20 mL of H₂O led to the immediate formation of the AgCl precipitate. After stirring for 2 h, the AgCl precipitate was filtrated. Addition of 1,4-bis(4-pyridyl)acetylene (L₄) (0.184 g, 1.02 mmol) to the filtrate and stirring overnight gave the white-yellow emulsion. After removal of volatiles, the resultant solid was dissolved in 2 mL of DMSO. The remaining AgCl was removed from the solution by centrifugation, and the resulting solution was filtered. Recrystallization from DMSO/acetone gave the single crystal of **4a·NO₃** (0.450 g, 0.284 mmol, 82.0% yield). IR (KBr, cm^{-1}) 3088 w, 2999 m, 2913 w (ν_{C-H}), 2093 br ($\nu_{C\equiv C}$), 1612 s ($\nu_{C=N}$), 1510 w, 1469 m, 1432 s ($\nu_{C=C}$), 1384 (ν_{N-O}), 1280 w, 1220 m, 1123 w, 1103 w, 1067 w, 1022 m, 954 m, 849 m, 810 m, 769 w, 707 w, 668 w, 582 w, 541 w, 410, w, 389 w, 341 w, 307 w, 280 w. ^{1}H NMR (270 MHz, DMSO-d_6) δ_H (ppm) 9.22 (d, $^2J = 5.9$ Hz, *Py*(α), **4b·NO₃**), 9.14 (d, $^2J = 6.5$ Hz, *Py*(α), **4a·NO₃**), 7.81 (*Py*(β), $^2J = 5.9$ Hz, **4b·NO₃**), 7.75 (*Py*(β), $^2J = 6.4$ Hz, **4a·NO₃**), 2.95 (*CH₂*), 2.59 (*Me*). ^{13}C{H} NMR (67.8 MHz, DMSO-d_6) δ_C (ppm) 151.37 (*Py*(α)), 131.94 (*Py*(ipso)), 128.98 (*Py*(β)), 92.24 (*C≡C*), 62.28 (*CH₂*), 50.22 (*Me*). Anal. Calcd. for $C_{86}Pd_4S_7H_{150}O_{37}N_{24}$ (**4a·NO₃·7DMSO·6H₂O**): C, 37.39; H, 5.47; N, 12.17; S, 8.12%. Found: C, 37.66; H, 5.58; N, 12.00; S, 8.27%.

Synthesis of [(en*)Pd(L₅)]$_m$(NO₃)$_{2m}$ (5a·NO₃ (m = 3), 5b·NO₃ (m = 4)). The reaction of (en*)PdCl₂ (0.316 g, 1.08 mmol) with 2 equiv of AgNO₃ (0.366 g, 2.15 mmol) in 20 mL of H₂O led to the immediate formation of the AgCl precipitate. After stirring for 2 h, the AgCl precipitate was filtrated. Addition of 1,4-bis(4-pyridyl)benzene (L₅) (0.250 g, 1.08 mmol) to the filtrate and stirring overnight gave the white-yellow emulsion. After removal of the volatiles, the resultant solid was dissolved in 2 mL of DMSO. The remaining AgCl was removed from the solution by centrifugation, and the resulting solution was filtered. The recrystallization from DMSO/acetone gave the single crystal of **5a·NO₃** (0.502 g, 0.289 mmol, 81.0% yield). IR(KBr, cm^{-1}) 3084 w, 2990 m, 2909 m (ν_{C-H}), 1613 s ($\nu_{C=N}$), 1486 m, 1469 m, 1435 s, 1384 vs (ν_{N-O}), 1226 m, 1125 w, 1027 m, 955 m, 824 m, 810 m, 769 w, 718 w, 705 w, 580 w, 505 w. ^{1}H NMR (270 MHz, DMSO-d_6) δ_H (ppm) 9.23 (d, $^2J = 5.4$ Hz, *Py*(α), **5b·NO₃**), 9.14 (d, $^2J = 6.2$ Hz, *Py*(α), **5a·NO₃**), 8.16 (d, $^2J = 5.4$ Hz, *Py*(β), **5b·NO₃**), 8.08 (d, $^2J = 6.2$ Hz, *Py*(β), **5a·NO₃**), 8.01 (s, C₆H₄, **5b·NO₃**), 7.94 (s, C₆*H₄*, **5a·NO₃**), 2.98 (s, *CH₂*), 2.61 (s, *Me*, **5a·NO₃**), 2.45 (s, *Me*, **5b·NO₃**). ^{13}C{H} NMR (67.8 MHz, DMSO-d_6) δ_C (ppm) 151.72 (*Py*(α)), 148.98 (**5a·NO₃**), 148.41 (**5b·NO₃**), 136.61 (**5a·NO₃**), 128.44 (*Py*(β)), 124.42 (**5a·NO₃**), 124.09 (**5b·NO₃**), 62.49 (*CH₂*), 50.87 (*Me*). Anal.

Calcd for $C_{68}Pd_3SH_{98}O_{23}N_{18}$ (**5a·NO₃·DMSO·4H₂O**): C, 43.28; H, 5.23; N, 13.36; S, 1.70%. Found: C, 43.05; H, 5.08; N, 13.04; S, 1.76%.

DFT Calculations. The DFT calculations were performed with the Gaussian 03 software.[45] The optimized structures of **na** and **nb** in solutions were obtained with the C-PCM calculation.[46] The calculated energies and properties depended much on the cavity sizes, and the data calculated with the UAHF cavity only reproduced the experimental data.[47] The boundary between the solute and solvent was defined as the solvent excluded surface area. The optimized structures of **na** and **nb** in water were obtained using 6-31G*/LanL2DZ hybrid basis sets with the B3LYP level of theory.[48−50] The single-point energy C-PCM calculations of **na** and **nb** in water, DMSO, and DMF were carried out using 6-31+G**/LanL2DZ hybrid basis sets with the B3LYP level of theory with UAHF parameters and the radius of palladium of 1.50 Å.[51] The parameters of DMF in ref 52 were used for the calculation. The chemical shifts of **na** and **nb** in DMSO were estimated using GIAO−DFT[53] with 6-31+G**/LanL2DZ hybrid basis sets with the B3LYP level of theory.

Supporting Information Available: Spectroscopic and crystallographic data, DFT calculation results, and complete ref 45. This material is available free of charge via the Internet at http://pubs.acs.org.

(45) Frisch, M. J. et al. *Gaussian03*, revisionD.02; Gaussian, Inc.: Wallingford, CT, 2004.

(46) (a) Tomasi, J.; Mennucci, B.; Cammi, R. *Chem. Rev.* **2005**, *105*, 2999. (b) Barone, V.; Cossi, M. *J. Phys. Chem.* **1998**, *A102*, 1995. (c) Cossi, M.; Rega, N.; Scalmani, G.; Barone, V. *J. Comput. Chem.* **2003**, *24*, 669.

(47) The $\Delta G°$ values calculated with the UA0 and UAKS cavities were quite different from those obtained experimentally.

(48) (a) Hehre, W. J.; Ditchfield, R.; Pople, J. A. *J. Chem. Phys.* **1972**, *56*, 2257. (b) Hay, P. J.; Wadt, W. R. *J. Chem. Phys.* **1985**, *82*, 270. (c) Hay, P. J.; Wadt, W. R. *J. Chem. Phys.* **1985**, *82*, 284. (d) Hay, P. J.; Wadt, W. R. *J. Chem. Phys.* **1985**, *82*, 299.

(49) Becke, A. D. *J. Chem. Phys.* **1993**, *98*, 5648.

(50) (a) Perdew, J. P.; Burke, K.; Ernzerhof, M. *Phys. Rev. Lett.* **1996**, *77*, 3865. (b) Perdew, J. P.; Burke, K.; Ernzerhof, M. *Phys. Rev. Lett.* **1997**, *78*, 1396.

(51) The Cambridge Structural Database (CSD) radius of palladium was taken from the website (http://www.ccdc.cam.ac.uk/products/csd/radii), and used to reproduce the $\Delta G°$ value for **2** in DMSO.

(52) Böes, E. S.; Livotto, P. R.; Stassen, H. *Chem. Phys.* **2006**, *331*, 142.

(53) (a) McWeeny, R. *Phys. Rev.* **1962**, *126*, 1028. (b) Ditchfield, R. *Mol. Phys.* **1974**, *27*, 789. (c) Dodds, J. L.; McWeeny, R.; Sadlej, A. J. *Mol. Phys.* **1980**, *41*, 1419. (d) Wolinski, K.; Hilton, J. F.; Pulay, P. *J. Am. Chem. Soc.* **1990**, *112*, 8251.